Journal of Quantitative Spectroscopy & Radiative Transfer 241 (2020) 106719

Contents lists available at ScienceDirect

Journal of Quantitative Spectroscopy & Radiative Transfer

journal homepage: www.elsevier.com/locate/jqsrt

Scattering of light by dense particulate media in the geometric optics regime

Timo Väisänen[a,*], Julia Martikainen[a], Karri Muinonen[a,b]

[a] Department of Physics, University of Helsinki, P.O. Box 64, 00014, Finland
[b] National Land Survey of Finland, Finnish Geospatial Research Institute (FGI), Geodeetinrinne 2, Masala 02430, Finland

ARTICLE INFO

Article history:
Received 1 July 2019
Revised 11 September 2019
Accepted 23 October 2019
Available online 24 October 2019

Keywords:
Geometric optics
Radiative transfer
Gaussian random sphere
Light scattering
Discrete random media
Dense media

ABSTRACT

We present a hybrid radiative transfer geometric optics approximation to model multiple light scattering in arbitrary finite discrete random media in the geometric optics regime. In the hybrid model, the medium is divided into a mantle composed of discrete particles and into a diffusely scattering core. In the mantle, multiple scattering is handled by using a ray-tracing algorithm with the generalized Snel's law for inhomogeneous waves, whereas, in the core, ray tracing with diffuse scatterers is incorporated to approximate multiple scattering and absorption. The extinction distances required to compute the scattering in the core are derived numerically by tracing the distances of the scattering and absorption events instead of using the classical extinction mean free path length. We have written a new framework that can treat arbitrary meshes consisting of watertight surface meshes with multiple diffuse scatterers and refractive indices. Comparison between the "ground truth" obtained from pure geometric optics ray tracing, the solutions obtained by using radiative transfer, and the hybrid model show that the hybrid model can produce better results, particularly, if a densely-packed medium is studied. In the future, the new approximation could be used to solve light scattering from larger media, such as asteroid surfaces, that are out of reach for the pure geometric optics methods due to their computational complexity.

1. Introduction

Light scattering in the geometric optics regime, where targeted objects are larger than the wavelength, has been under extensive study for a long time ranging from the field of astrophysics [1–3] to the field of atmospheric sciences [4]. The research is being continued by, e.g., improving the models [5–7] and studying various effects derived from the approximations [8]. The simplest way to approximate light scattering in the geometric optics regime is to use ray-tracing algorithms [9]. When interacting with the surfaces, the rays can be refracted or reflected according to the Fresnel equations and Snel's law in weakly absorbing media, whereas more generalized forms of these are required when a high imaginary part of the refractive index is present [10–12]. Due to the simplicity of the algorithm, it is an excellent way to simulate light scattering of complex-shaped particles, but if the studied object is vast with multiple facets the required computing capacity can grow tremendously. The options are then to use approximations or increase the computing capacity. Approximations vary from applying shadowing to the surface [13] or using radiative transfer to approximate the multiple scattering part of the problem [4]. There are also related works about shadowing and surface roughness such as [14–16].

Recently, radiative transfer in the geometric optics regime was used to model multiple scattering in dense regoliths of the asteroid (4) Vesta using the ray-tracing program SIRIS4 [17–20] with diffuse scattering and inhomogeneous-wave capabilities. In that approach, multiparticle systems are studied by computing the scattering properties of multiple particles independently, mixing them statistically and using the ensemble-averaged scattering characteristics as a diffuse scatterer. In order to improve the usage of radiative transfer with materials such as densely-packed regoliths, we rewrote the existing SIRIS4 framework to support multiple particles. The new framework was written to be the general version of SIRIS4, capable of handling any triangulated meshes consisting of watertight (or closed) surface meshes, support multiple complex refractive indices and diffuse materials instead of being bound to Gaussian-random-sphere particles. Furthermore, a packing algorithm capable of producing meshes composed of multiple particles and shapes had to be written. The framework will be used

* Corresponding author.
E-mail address: timo.h.vaisanen@helsinki.fi (T. Väisänen).

https://doi.org/10.1016/j.jqsrt.2019.106719

to compare the model, in which radiative transfer is applied, to the ground truth, where everything is computed rigorously using purely geometric optics laws.

To model large media, such as planetary regoliths, more accurately, we present a hybrid radiative transfer geometric optics approximation (from now on a hybrid model), in which a medium is divided into a mantle of discrete particles and a diffusely scattering core. The extinction distances in the core are drawn from a numerically acquired distribution of extinction distances instead of using a classical extinction mean free path length based on the sparse-medium approximation. We show numerically that the hybrid model with the extinction distance distribution is capable of solving a full scattering matrix more accurately than the pure radiative transfer (RT) approach when the medium is dense. The comparison is performed by solving the multiple scattering problem rigorously with the generalized laws by Snel and Fresnel, the RT approach, and the hybrid model.

In the Theory section, we present the major terminologies and concepts briefly, whereas, in the Methods section, the used methodologies (packing algorithm, SIRIS4, RT, hybrid model) are described more closely. In the Results and Discussion, these different methodologies are compared against each other by studying different discrete random media.

2. Theory

Electromagnetic scattering can be divided into six different regimes, which identify available scattering theories to solve the light scattering problem [21]. The regimes are distinguished by the size parameter x and the real part of the refractive index $\mathrm{Re}(m)$. The size parameter is a relation between the radial measure of the particle a and the wavelength of the incident light λ ($k = 2\pi/\lambda$ is the wave number),

$$x = ka = \frac{2\pi a}{\lambda}. \tag{1}$$

If the refractive index is intermediate ($\mathrm{Re}(m) \approx 1.5$), there are roughly three regimes; the Rayleigh ($x \ll 1$), Mie/resonance ($x \approx 1$), and geometric optics ($x \gg 1$) regimes. The imaginary part of the refractive index presents the absorptive properties of the material.

Following the formalism of [22], electromagnetic scattering can be described with the relation

$$\mathbf{I}_{\mathrm{sca}} = \frac{1}{k^2 r_d^2}\mathbf{S}(\theta)\mathbf{I}_{\mathrm{inc}}, \tag{2}$$

in which the Stokes vectors $\mathbf{I}_{\mathrm{inc}}$ and $\mathbf{I}_{\mathrm{sca}}$ can be used to describe the polarization state of the incident and scattered electromagnetic wave with the help of the scattering matrix $\mathbf{S}(\theta)$ and the distance r_d. By integrating over the full solid angle, the scattering cross section σ_{sca} is attainable,

$$\sigma_{\mathrm{sca}} = \frac{1}{k^2}\int_{4\pi} d\Omega\, \mathbf{S}_{11}(\theta), \tag{3}$$

which, with the radiation absorbed by the particle σ_{abs} (absorption cross section), can be used to find the extinction cross section

$$\sigma_{\mathrm{ext}} = \sigma_{\mathrm{sca}} + \sigma_{\mathrm{abs}}. \tag{4}$$

These can be used to find the single-scattering albedo $\tilde{\omega}$,

$$\tilde{\omega} = \frac{\sigma_{\mathrm{sca}}}{\sigma_{\mathrm{ext}}}, \tag{5}$$

and the so-called co-albedo $1 - \tilde{\omega}$ describing the fraction of absorbed light.

The light scattering characteristics in the geometric optics regime can be approximated by tracing independent parallel rays because the electromagnetic waves act as a localized entity due to the size difference of the surface and the wavelength ($\lambda \ll a$) [23]. This approximation is still missing forward diffraction, which is caused by the electromagnetic wave collectively interacting with the apertures and exterior of the medium. Fortunately, the forward diffraction can be treated as a separate entity in the geometric optics regime [17,24]. The scattering cross section σ_{sca} as well as $\mathbf{S}$ can be divided into the geometric optics (superscript GO) and forward diffraction components (superscript D)

$$\sigma_{\mathrm{sca}} = \sigma_{\mathrm{sca}}^{\mathrm{GO}} + \sigma_{\mathrm{sca}}^{\mathrm{D}} \tag{6}$$

and

$$\mathbf{S}(\theta) = \mathbf{S}^{\mathrm{GO}}(\theta) + \mathbf{S}^{\mathrm{D}}(\theta). \tag{7}$$

The forward diffraction is only prominent near the forward-scattering direction and can be omitted if only the scattered light in the backscattering direction is studied, which is the case in this study. The geometric optics treatment can be studied further from [17,19].

For the RT approach, the extinction coefficient is defined by

$$\kappa_{\mathrm{ext}} = \frac{\sigma_{\mathrm{ext,v}}}{V}, \tag{8}$$

in which $\sigma_{\mathrm{ext,v}}$ gives the total extinction cross section of the scatterers within a volume element V. It can be then used to find the rate of which the ray loses intensity within the media, and define the extinction mean free path length ℓ_0,

$$\ell_0 = \frac{1}{\kappa_{\mathrm{ext}}}, \tag{9}$$

which is the average distance between extinction events.

3. Methods

3.1. Random media generation

Multiparticle ray-tracing simulations require the generation of the geometry for the object. One way is to generate multiparticle meshes with the so-called Gaussian random field particles [25] but in this study, we are interested in the usage of the Gaussian-random-sphere (from now on GRS) particles [17] as the shape of the individual particle, so a packing program was written. A mesh composed of GRS particles with a relatively small standard deviation of the radius, and a thin size distribution are easily obtainable up to the volume fraction v=0.3 by randomly placing the particles. A wider size distribution, more exotic shapes, or higher densities require more sophisticated algorithms to obtain the desired random media. To be able to generate meshes with volume fraction up to 0.4 or higher, a simplified version of the so-called mechanical contraction was implemented [26–28].

In the algorithm, the size distribution is generated before the packing starts, and the large particles are placed before the small ones to ensure that every particle is placed inside the periodic box. The medium is initially packed by randomly placing randomly-oriented particles in a way that they do not overlap with each other which is possible up to v=0.3. In the next step, the positions of the particles are scaled by the factor of Λ while the original shape, orientation, and size are kept constant. Simultaneously, the periodic boundaries are only scaled by a factor of $(1 + \Lambda) \cdot 0.5$ and all the particles are translated toward the center of the periodic box. The shrinking is followed by a relaxation process in which the overlapping particles are identified, and a displacement factor $\Delta\vec{x}_i$ is computed from

$$\vec{o}_i = \sum_j^{N_i} \frac{\vec{r}_i - \vec{r}_j}{|\vec{r}_i - \vec{r}_j|^2},$$

$$\Delta\vec{x}_i = \frac{\vec{o}_i}{|\vec{o}_i|} u \Delta x, \tag{10}$$

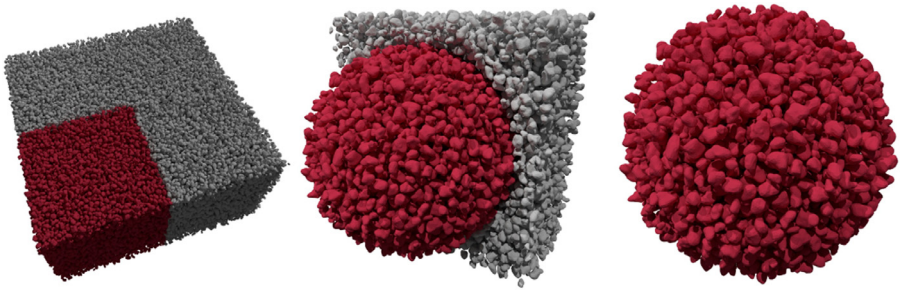

Fig. 1. Random medium composed of Gaussian random spheres with a Gaussian size distribution (left). The single periodic box is highlighted in red. Spherical medium (red) is culled from the periodic box (middle). An example of a spherical medium used in the simulations (right). (For interpretation of the references to colour in this figure legend, the reader is referred to the web version of this article.)

in which N_i is the number of particles, which overlap with the particle i, u=[0,1[is a uniform random number, Δx is the maximum translation length and $\vec{r}_k$ is the location of the particle k. The displacements are then applied to the particles. After all the translations are executed, particles are randomly selected one by one and allowed to translate and rotate randomly while preventing new overlapped particles from forming. This relaxation is executed multiple times until there are no overlapping particles, and after that, the particles are allowed to move while the non-overlap condition is enforced. The system can be shrunk and relaxed multiple times in small steps which gradually reduces the volume fraction of the periodic boundary to the desired value.

The packer is written in C++ and it uses the Flexible collision library [29] to detect the intersecting facets of arbitrary triangle meshes. Because the collision is based on the intersection of the facets, a particle shape is not enough to enforce the non-overlap condition, and hence internal structure needs to be generated for the particle (e.g., Voronoi) especially if the radii of the meshes follow a size distribution, such as the power-law distribution. The program generates a mesh which then can be culled from the periodic box to the desired shape, such as a sphere (See Fig. 1). Particles can be scaled to follow a size distribution. The user provides a discrete distribution $r(u)$ of radii of spheres, and the given meshes with volumes V_i are scaled with a factor of

$$\Xi_i = \sqrt[3]{\frac{\frac{4}{3}\pi r(u)^3}{V_i}}, \tag{11}$$

to give an equal-volume sphere.

3.2. New framework

In the new framework for SIRIS4 [18–20], most underlying elements are the same as earlier [19,20]. However, there are minor changes which have been introduced to parts handling the physics since the original publications [19,20]. The high imaginary part of the refractive indices would break the energy conservation and therefore the deflection angle was added [10,30]. However, it added another shortcoming since the new framework uses a Mueller matrix to relate the polarization of the incoming and emerging rays. Problems emerge with the surface rays, which are refracted close to the surface. These rays emerge from the generalized Snel's law when in the classical sense a total internal reflection occurs. In order to detect the emergence of the surface rays, we use the condition from Snel's law for the non-absorbing case,

$$\frac{n_1 \sin\theta_i}{n_2} > 1, \tag{12}$$

instead of the one derived for the generalized Snel's law [12] for inhomogeneous waves,

$$\frac{N_1 \sin\theta_i}{N_2} > 1, \tag{13}$$

in which N_1 and N_2 are the real parts of the apparent complex refractive indices. The user is made aware of the collected energy from the surface rays at the end of the program execution.

The SIRIS4 generated only a single GRS particle at a time. SIRIS4 had to be reworked to support arbitrary meshes and various materials with or without diffuse inclusions in order to accomplish the research of this paper. The new framework is written in C++, and the rays are traced in an axis-aligned bounding box (AABB) tree using the Computational Geometry Algorithms Library (CGAL) [31]. The refraction, reflection, and radiative transfer are handled with the Fortran modules presented in SIRIS4 [19,20] excluding the changes mentioned above. The new framework is not capable of producing averaged values over multiple meshes so these features need to implemented with separate scripts, e.g., by invoking the program with multiple meshes.

3.3. Radiative transfer approach

Large aggregates of particles in the geometric optics regime have been approximated by treating discrete scatterers as a diffuse scatterer and solving the light scattering properties by using radiative transfer [20]. First, the properties of individual scatterers are computed individually and the mixture is statistically combined to create one diffuse scatterer with collective properties such as a single extinction mean free path length ℓ, albedo $\tilde{\omega}$, and scattering matrix $\mathbf{S}$. The extinction coefficient for the mean free path length (see Eq. (9)) is solved by using the equation from [32],

$$\kappa_{\mathrm{ext,tot}} = n_0 \sum_{i=0}^{N} w_i \frac{\langle q_{\mathrm{ext}} A \rangle_i}{V_i}, \sum w_i = 1, \tag{14}$$

in which i presents an ensemble-averaged random particle with common properties, such as size, shape, and material composition, w_i is the weighting factor in the mixture, which corresponds to the underlying size distribution of the particles, $\langle q_{ext} A \rangle_i$ is the averaged extinction cross section of the scatterer, and V_i is the volume of the scatterer. The albedo $\tilde{\omega}$ is computed from the equation

$$\tilde{\omega} = \frac{\sum_{i=0}^{N} w_i \langle q_{\mathrm{sca}} A \rangle_i}{\sum_{i=0}^{N} w_i \langle q_{\mathrm{ext}} A \rangle_i}, \tag{15}$$

and the scattering matrix elements S_{11}, S_{12}, S_{22}, S_{33}, S_{34}, and S_{44} from

$$S_{lj} = \sum_{i=0}^{N} w_i S_{lj,i}. \tag{16}$$

After the collective properties are computed, the polygonal mesh corresponding to the studied aggregate is used as a host for the

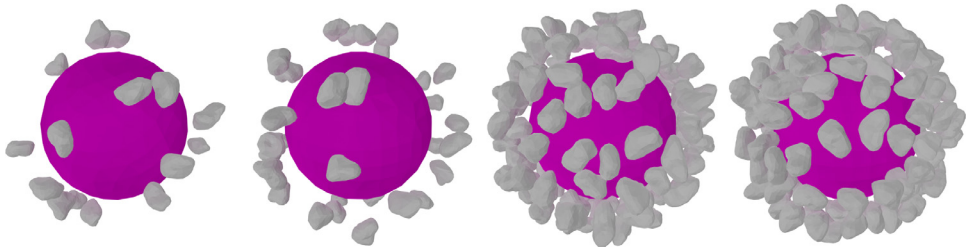

Fig. 2. The diffusely scattering core (purple) and the pure geometric optics mantle (grey) for the volume fractions v= 0.05, 0.1, 0.3, and 0.4. (For interpretation of the references to colour in this figure legend, the reader is referred to the web version of this article.)

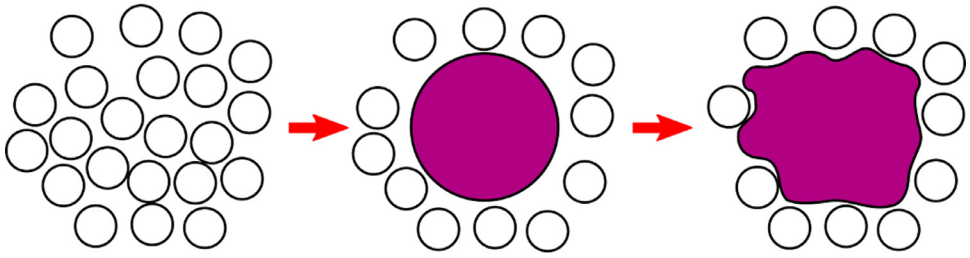

Fig. 3. The mantle and the core are created by removing inner particles (white) from the packed medium and by placing a spherical core (purple) to the center. The gap between the core and the mantle is filled by "inflating" the core. (For interpretation of the references to colour in this figure legend, the reader is referred to the web version of this article.)

diffuse scatterers, and the scattering properties are solved by using radiative transfer [18,33,34].

If the studied media is small and the extinction mean free path length is large, it is probable that the ray propagates through the media without interaction, which is then registered in the forward scattering direction. The direct transmission in the radiative transfer approach is equivalent to no interaction in the pure geometric optics approach causing absolute values to differ. Therefore, in order to make the results comparable, effective cross section area A_{eff} is used instead of the geometrical cross section area A_{geom} when diffuse scattering is in use. The effective cross section area is defined as

$$A_{\mathrm{eff}} = A_{\mathrm{beam}} \frac{n_{\mathrm{hit}} - n_{\mathrm{dt}}}{n}, \tag{17}$$

whereas the geometrical cross section is

$$A_{\mathrm{geom}} = A_{\mathrm{beam}} \frac{n_{\mathrm{hit}}}{n}, \tag{18}$$

in which A_{beam} is the cross section of the incident beam, n is the total number of generated rays of which n_{hit} and n_{dt} hit the medium, the latter being directly transmitted.

3.4. Hybrid model and extinction distance distribution

The RT is derived for small particles, as well as sparse infinite media [23], and if the RT is applied to the densely-packed discrete random media, there will be problems. They arise from the replacements of the discrete surface with a statistical layer without distinct features such as shadows.

Distinct surface features are not present in the pure RT approach. Surface features are essential especially when the medium is opaque due to scattering being localized near the boundary instead of penetrating deep into the medium. In the hybrid model, the surface structure is added by leaving a layer of particles (mantle) on the surface of the RT region (see Fig. 2), in which the generalized Snel's law applies. We used the packing algorithm mentioned above to generate fully packed meshes from which the mantle is formed by culling inner and outer particles. The RT region or a core is then placed at the center of the mantle (see Fig. 3). In order to prevent a massive gap between the mantle and the core, the gap is filled by "inflating" each facet of the core by scaling the vertices while preventing overlaps forming.

Another problem in the RT is the simplified extinction mean free path length based on the geometries. Fig. 4 demonstrates the discrepancies caused by the use of a diffuse scatterer as an approximation for the finite-sized aggregates. For the RT ray (blue line), the scattering event occurs in an arbitrary location described by the exponential distribution along the line of the propagation, then absorption is applied, and the ray is scattered to a new direction, whereas the real interaction is more complex with multiple refractions and reflections (see rays a, b, and c). Eq. 9 does not include shape information, shadowing from other particles or light scattering properties of a single particle. Hence, we propose that, in order to remove the discrepancy between the hybrid model and the RT, the distance to the next scatterer is drawn from an extinction distance distribution, which removes the need for the exponential attenuation assumption.

We decouple the extinction distances from the actual scattering and absorption processes. For the latter two processes, we assign the average single-particle characteristics. The extinction distance distribution can be generated in a separate step before the actual simulation by using the same meshes. The ray is traced through the first particle without interacting with it (purple lines Fig. 4), and then the distance (red lines) to the first reflection (ray a), full absorption (ray b), or the first refraction out from the particle (ray c) is logged. Next, the logged distances are used to form a probability density function. The right tail of the distribution may need to be extrapolated if the right end of the distribution is cut due to the small size of the medium. These distributions can then be used to draw distances between interactions in the diffuse medium.

Earlier work in [15,16,35] suggests that separating the average scattering matrix from the extinction distances can lead satisfactory approximations.

4. Results

The scattering properties of discrete random media were computed using five different ways, the pure geometric optics (GO) representing the ground truth (see Figs. 6–13). This approach is then compared to the RT solution and the hybrid model by us-

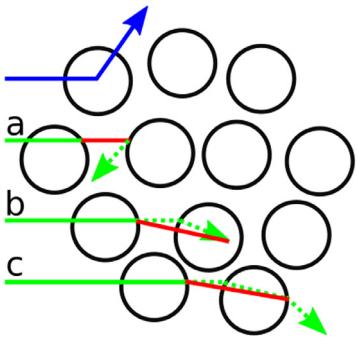

Fig. 4. A demonstration of a problem of the extinction distances in the RT approach (blue arrow) compared to the pure geometric optics approach (rays a, b, c). In the latter, the extinction distances (red) are computed by letting the rays pass through the first particle without interaction (magenta), and then the rays are traced until they are reflected (a), absorbed (b), or refracted from a particle (c). In (c), the ray may undergo multiple internal reflections before the refraction. (For interpretation of the references to colour in this figure legend, the reader is referred to the web version of this article.)

ing the classical extinction mean free path length ("diffuse, classic", "hybrid, classic") and the extinction distance distribution ("diffuse, eGO", "hybrid, eGO", e stands for the case, where the extinction distance distribution is computed using the GO.).

The studied media were composed of 100 GRS particles with a power-law index 4.0, relative standard deviation σ=0.2, and with refractive index m=1.6+i0.0001 generated by using the algorithm from [17]. The sizes of the particles were scaled to have the equal-volume-sphere radii that follow the power-law size distribution (index $\nu = 3$, x=[50,200], see Figs. 6–9) or to have constant size (x=200, see Figs. 10–13). The size of the medium was kept constant at kR=2000, whereas the volume fraction varied among v=0.05, 0.1, 0.3, and 0.4. For the pure GO approach, the meshes were generated by using the algorithm described above in Section 3.1. The incident field covered a small area of the medium in order to minimize the effects of curvature (kR_{inc}=250) and the scattering angles 90°–180° are shown to highlight the differences in the backscattering direction. In Fig. 14, the distinctive differences of Figs. 9 and 13 are compared by showing the entire scattering angle range.

The extinction distance distributions are computed by using a modified version of the new framework, which logs distances between the scatterings and absorptions (see Section 3.4). Geometries used in this computation are the same as those used for the pure GO approach as an input, but the beam size is focused in the center of the studied medium kR_{inc}=50 to prevent effects from the curvature. Extinction distance distributions for the sparse cases (v=0.05 and v=0.1) were created using larger media kR_{inc}=8000, so that the entire right tail of the histogram could be obtained (see Fig. 5) . Exponential functions were fitted to the histograms in order to provide a comparison to the extinction mean free paths (see in Table 1).

The mantle and core were generated for the hybrid model by following the procedure discussed in Section 3.4. The mantle was created by removing particles whose centers coincide inside the sphere of radius $kR_{\mathrm{core,remove}}$=1400. Then the core ($kR_{\mathrm{core,init}}$=1200) was placed inside the mantle, and the gaps were filled by scaling vertices of the core's facets up to $kR_{\mathrm{core,inflated}}$=1600 if possible. The thickness of the mantle varied between kR_{crust}=[400,800]. Fig. 15 shows the effect of the gap to the results shown in Fig. 11.

In the RT approach (Section 3.3), the scattering properties of these 100 particles were computed individually using the framework, and were then used to form the collective scattering properties, albedo, extinction mean free path length (see Table 1), and

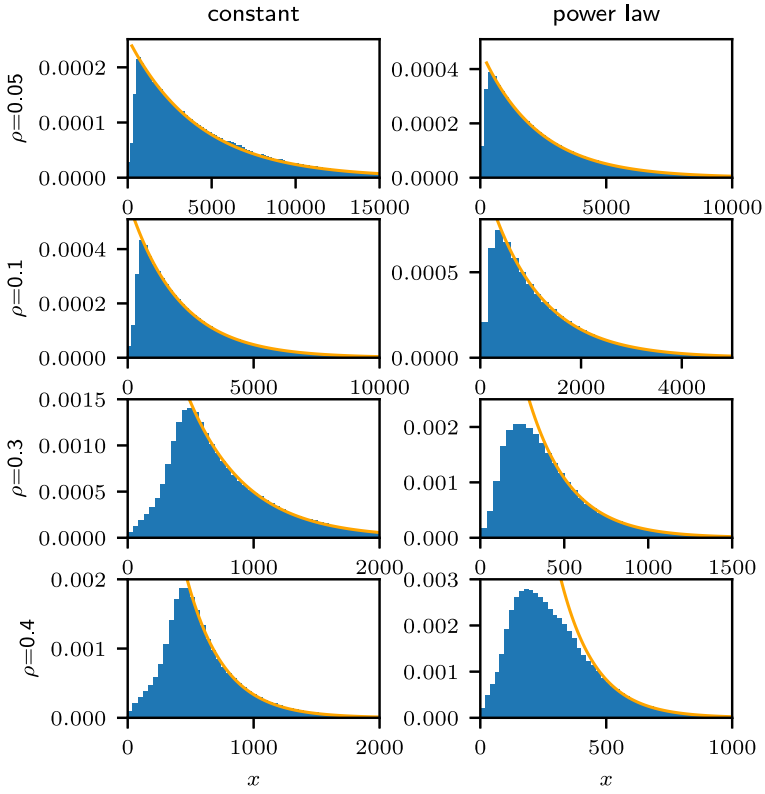

Fig. 5. Histograms for m=1.6+0.i0001 cases obtained by logging distances (x-axis) between the ray's entry point and the first refraction, reflection, or absorption point (see Fig. 4). The exponential attenuation function is fitted to the data to extrapolate the tail of the distribution (orange).

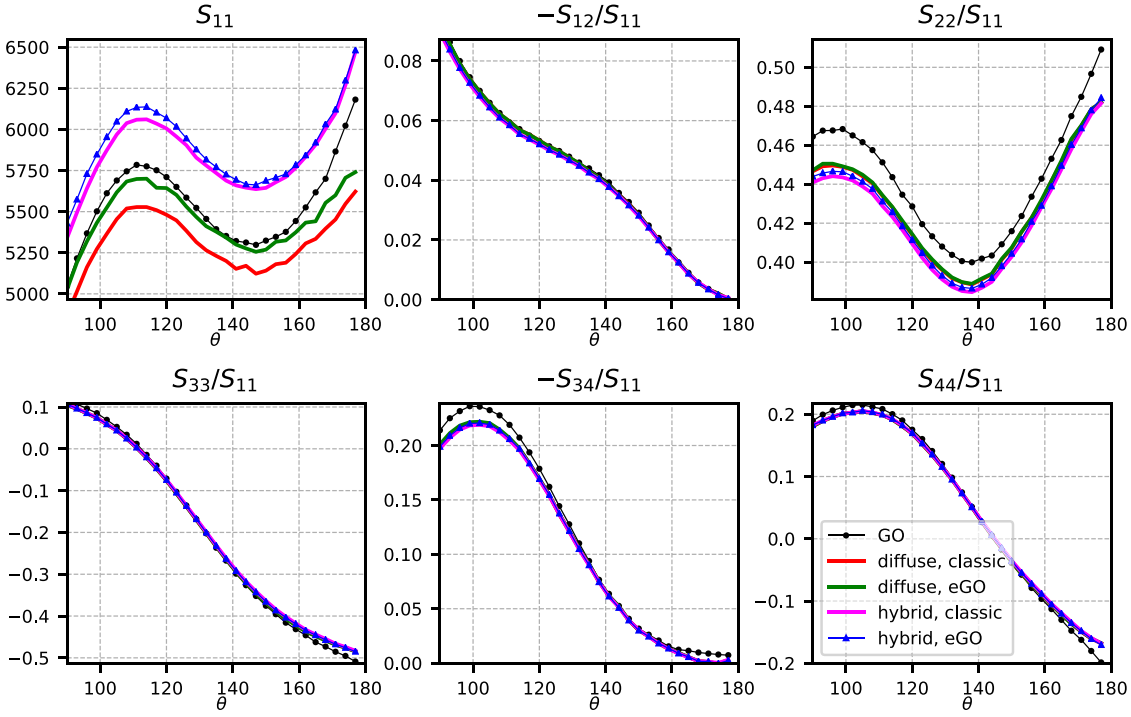

Fig. 6. Nonzero scattering matrix elements for an aggregate with v=0.05 and m=1.6+i0.0001 in the case of constant particle size.

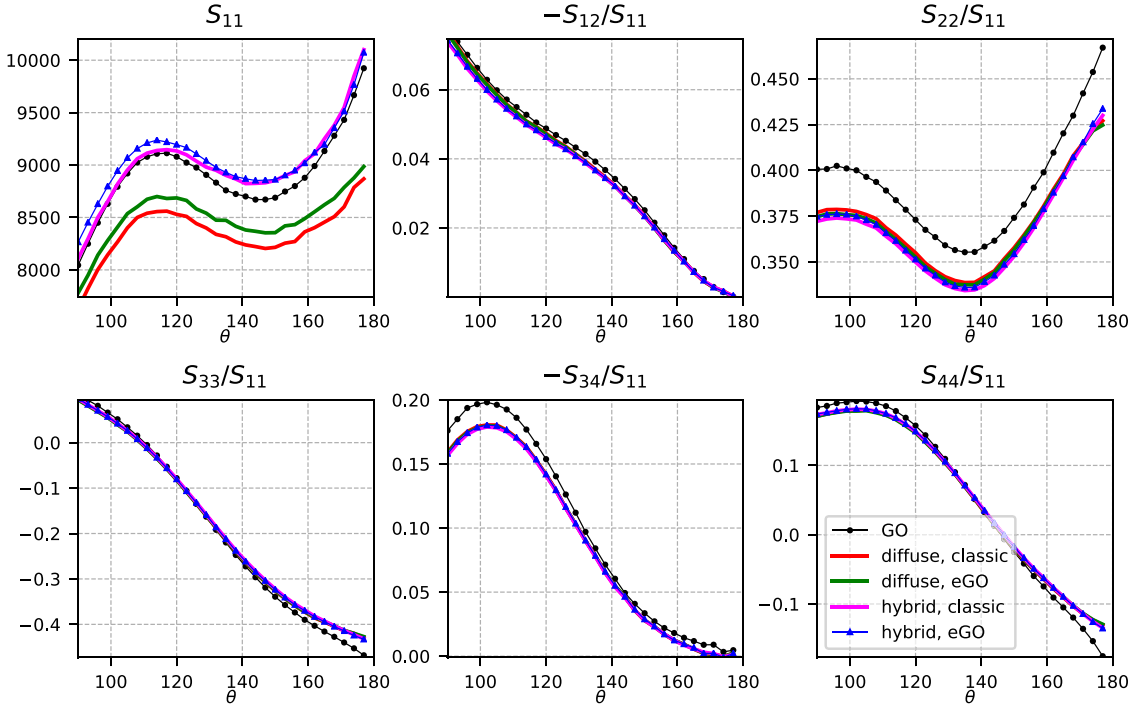

Fig. 7. Same as Fig. 6, but v=0.1.

scattering matrix by using the equations from Section 3.3. These collective properties were then input to the framework as a diffuse scatterer inside a spherical medium of size kR=2000. In addition, the mean free path length was replaced with the extinction distance distribution.

The albedos $\tilde{\omega}$ of each case are shown in Tables 2 and 3 alongside the mean absolute percentage error Δ for the angles between 0° and 180°.

5. Discussion

Figs. 6–13 show that the classical RT approach does not work when the medium is dense and contains complex size distributions. The best match acquired with the classical way is when the particles have a constant size and the medium is sparse (see Fig. 6). However, if the power-law distribution is present (see Fig. 10), the classical way exaggerates the number of multiple scat-

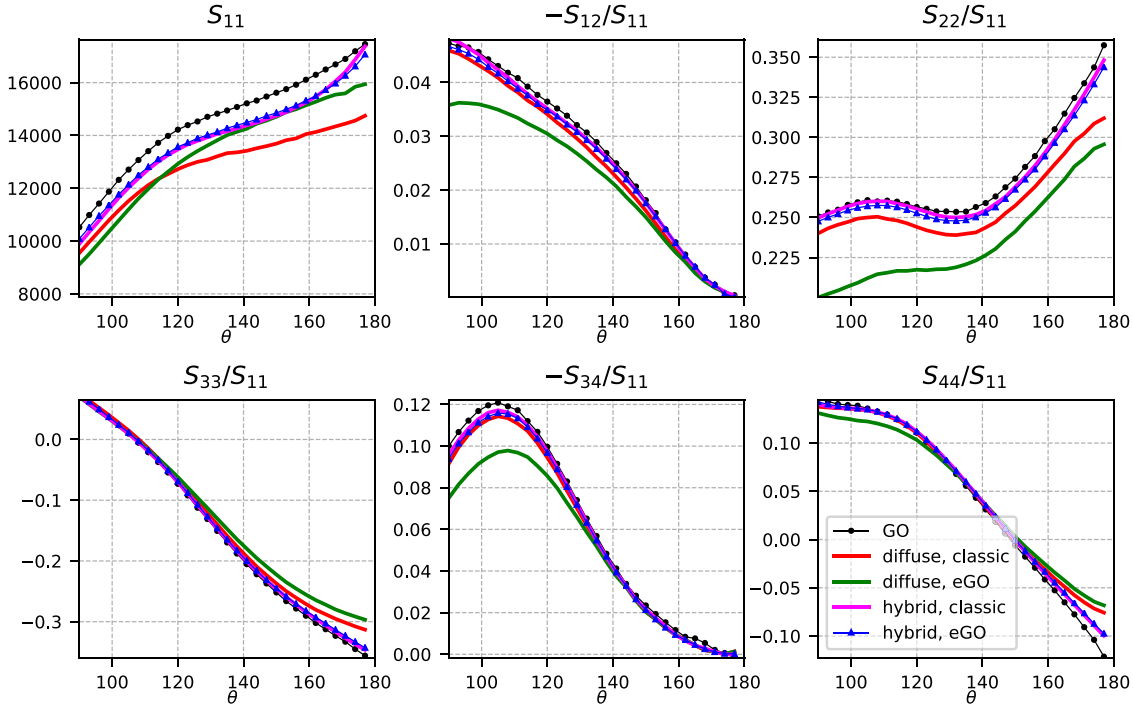

Fig. 8. Same as Fig. 6, but v=0.3.

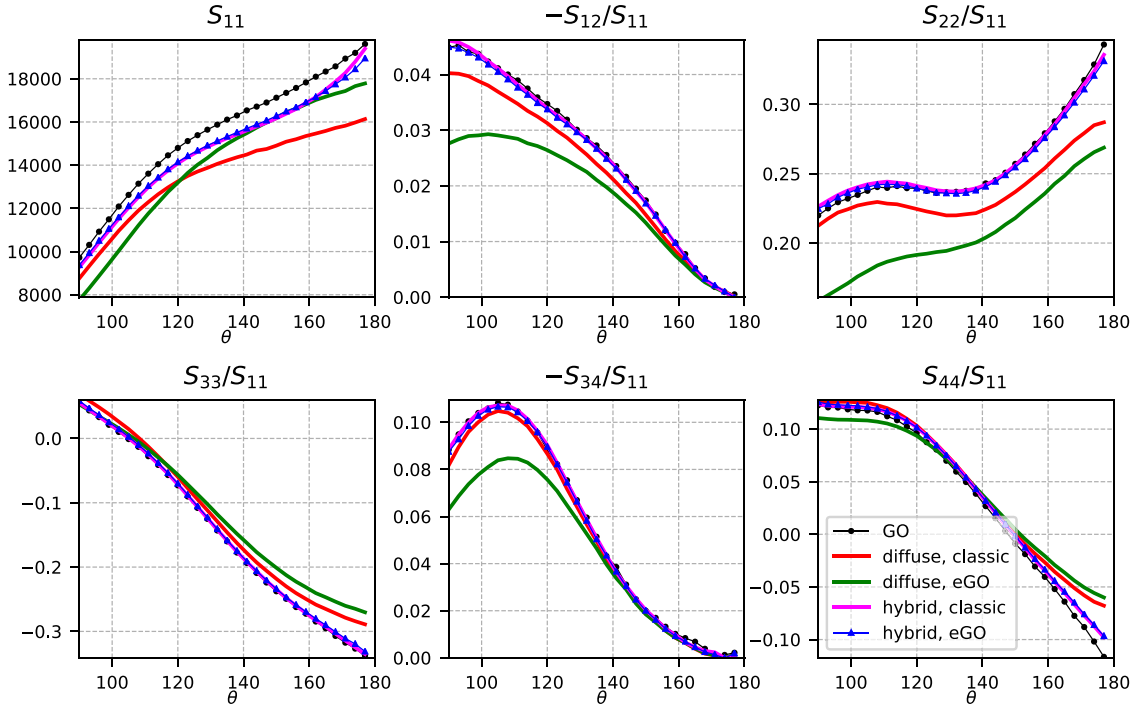

Fig. 9. Same as Fig. 6, but v=0.4.

tering events, which is shown as the lower mean free path length ℓ_0 in Table 1.

The intensity in the sparse cases (Figs. 6–7 and 10–11) can be improved by applying the correct extinction distance distribution, which is also supported by the values of Δ in Tables 2 and 3. The most notable improvements are with the power-law distributions because the computational distributions account for the shape difference of the particles (see Figs. 10–13). By comparing the scattering elements S_{12}, S_{22}, S_{33}, S_{34}, and S_{44}, it is clearly visible that the pure RT approach is not enough and, by adding a mantle of discrete particles, the discrepancies between the RT and GO can be corrected. The small discrepancy between the methodologies shows that surface structure and shadowing cannot be omitted when the medium is dense, and hence, the hybrid model should be used. In the dense cases ($v \geq 0.3$) the extinction distance correction seems to work but it is the degree of linear polarization ($-S_{12}/S_{11}$) and the depolarization (S_{22}/S_{11}) that reveal an even worse match with the "ground truth", and even the hybrid model

Table 1
16 different extinction mean free path lengths obtained by fitting an exponential function to the data in Fig. 5(orange line), compared to the extinction mean free path lengths ℓ_0 obtained by using Eq. (14).

v	Particle sizes	eGO	ℓ_0
0.05	constant	4239.0	4813.1
0.1	constant	1990.0	2406.5
0.3	constant	470.0	802.2
0.4	constant	292.0	601.7
0.05	power law	2248.0	1499.3
0.1	power law	1049.4	749.7
0.3	power law	254.5	249.8
0.4	power law	146.3	187.4

Table 2
The single-scattering albedos $\tilde{\omega}$ and the mean absolute percentage errors Δ for Figs. 6–9(constant particle size, m=1.6+i0.0001). Diffuse method is abbreviated by "diff", hybrid method by "hyb" and the usage of the classic extinction mean free path by "c".

	GO	diff, c		diff, eGO		hyb, c		hyb, eGO	
v	$\tilde{\omega}$	$\tilde{\omega}$	Δ (%)	$\tilde{\omega}$	Δ (%)	$\tilde{\omega}$	Δ (%)	$\tilde{\omega}$	Δ (%)
0.05	0.87	0.87	5	0.86	1	0.87	4	0.86	6
0.1	0.84	0.82	6	0.82	4	0.82	3	0.82	3
0.3	0.70	0.66	16	0.63	8	0.67	7	0.67	4
0.4	0.65	0.60	17	0.56	13	0.62	8	0.62	4

with the classical mean free path length is able to outdo the diffuse model.

Although the hybrid model with the extinction distance distribution seems to work in the dense cases (Figs. 8–9 and 12–13), similar results can be obtained by using the hybrid model with the classical extinction mean free path lengths. This is strong evidence for the surface roughness being the most important contributing factor to the outcome. This is also shown in the Δs of Tables 2 and 3 which indicate that the classic and eGO are both good. The small discrepancies are due to convergence problems, which are indicated by small fluctuations in the forward scattering direction (see Fig. 14). Another possibility is to study the entire scattering angle range in Fig. 14, which shows that even though the backscattering might be correct, the forward scattering might not be. This is probably due to holes in the mantle because the thin mantle of equisized particles can have large holes, as shown in Fig. 2. This would imply that if the mantle is thick enough, the underlying extinction rule can have inaccuracies. This is not surprising because the scattering in the thick opaque mantle dominates the scattering in the core.

The hybrid model results can be improved by adjusting the size of the inflated RT core, as is shown in Fig. 15, in which the inflated core is compared against the spherical core that would result in a gap between it and the mantle. Fig. 15 shows that by making the

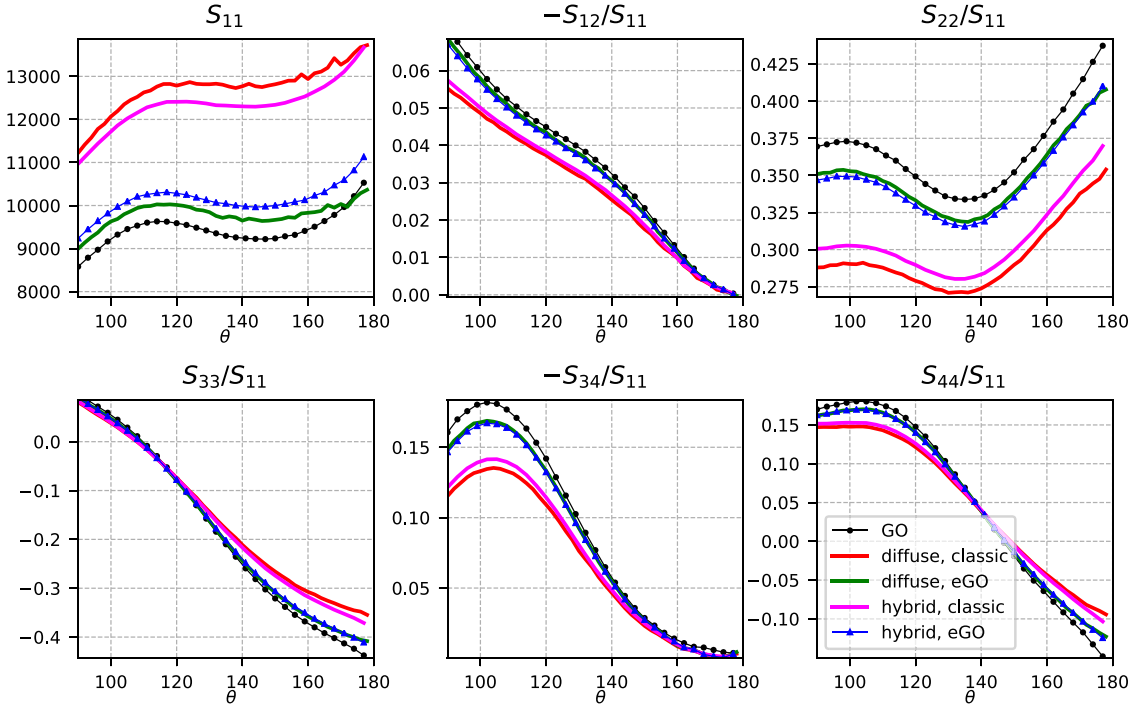

Fig. 10. Nonzero scattering matrix elements for an aggregate with v=0.05 and m=1.6+i0.0001 in the case of a power-law size distribution of particles.

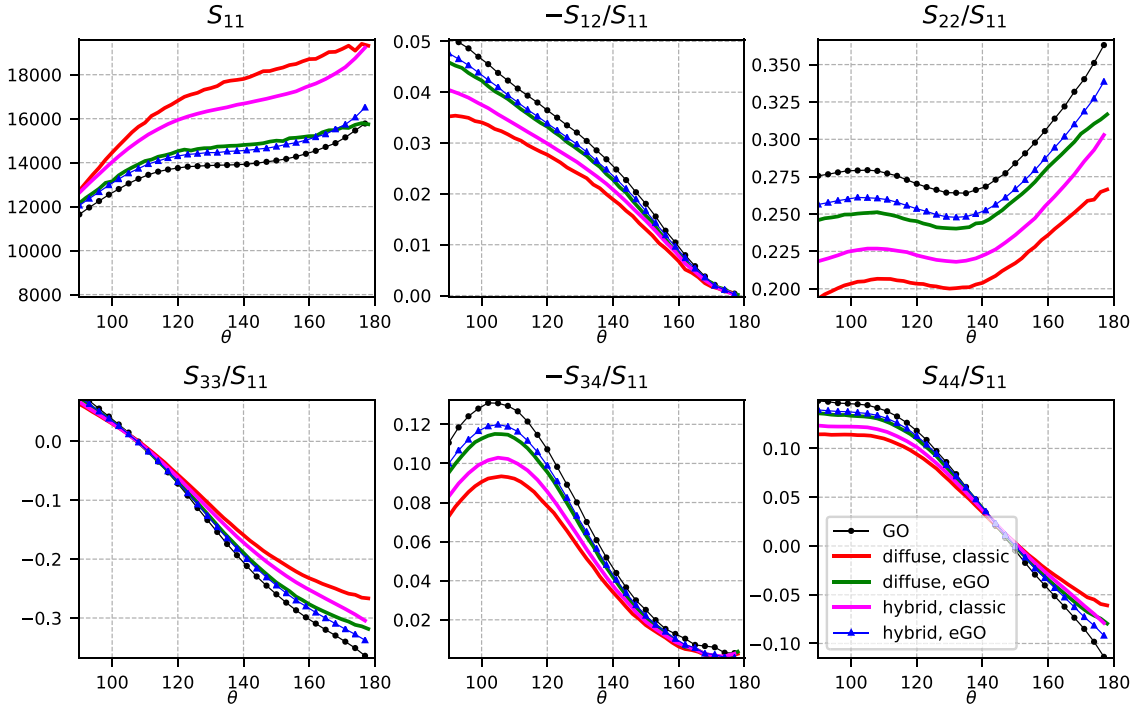

Fig. 11. Same as Fig. 10, but v=0.1.

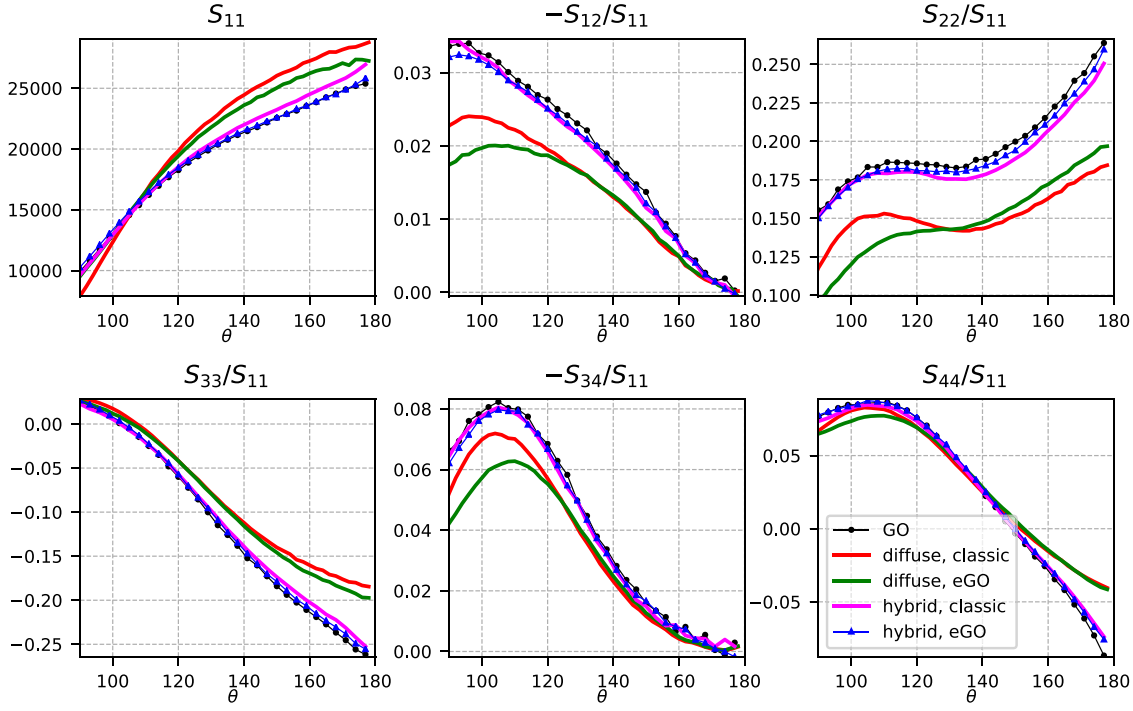

Fig. 12. Same as Fig. 10, but v=0.3.

Table 3
Same as Table 2, but for Figs. 10–13(power-law size distribution).

	GO	diff, c		diff, eGO		hyb, c		hyb, eGO	
v	$\tilde{\omega}$	$\tilde{\omega}$	Δ (%)	$\tilde{\omega}$	Δ (%)	$\tilde{\omega}$	Δ (%)	$\tilde{\omega}$	Δ (%)
0.05	0.91	0.86	28	0.94	4	0.91	25	0.92	6
0.1	0.87	0.86	25	0.90	4	0.85	20	0.89	4
0.3	0.73	0.70	30	0.75	7	0.71	12	0.74	6
0.4	0.67	0.66	31	0.70	12	0.66	9	0.68	10

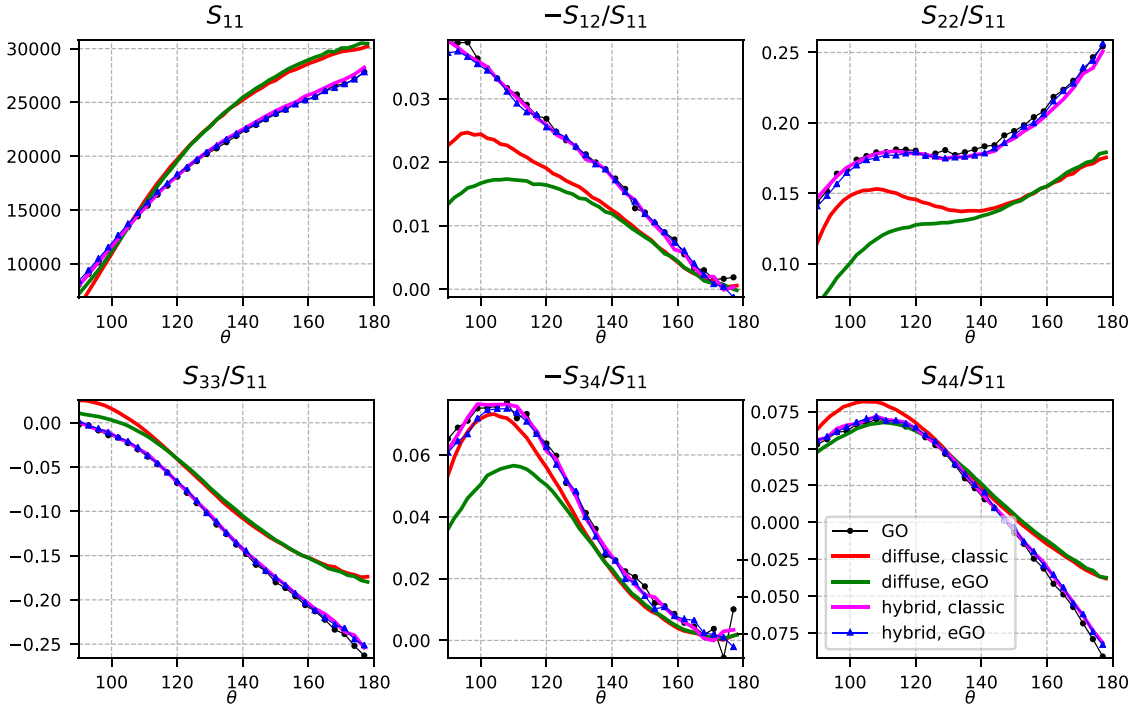

Fig. 13. Same as Fig. 10, but v=0.4.

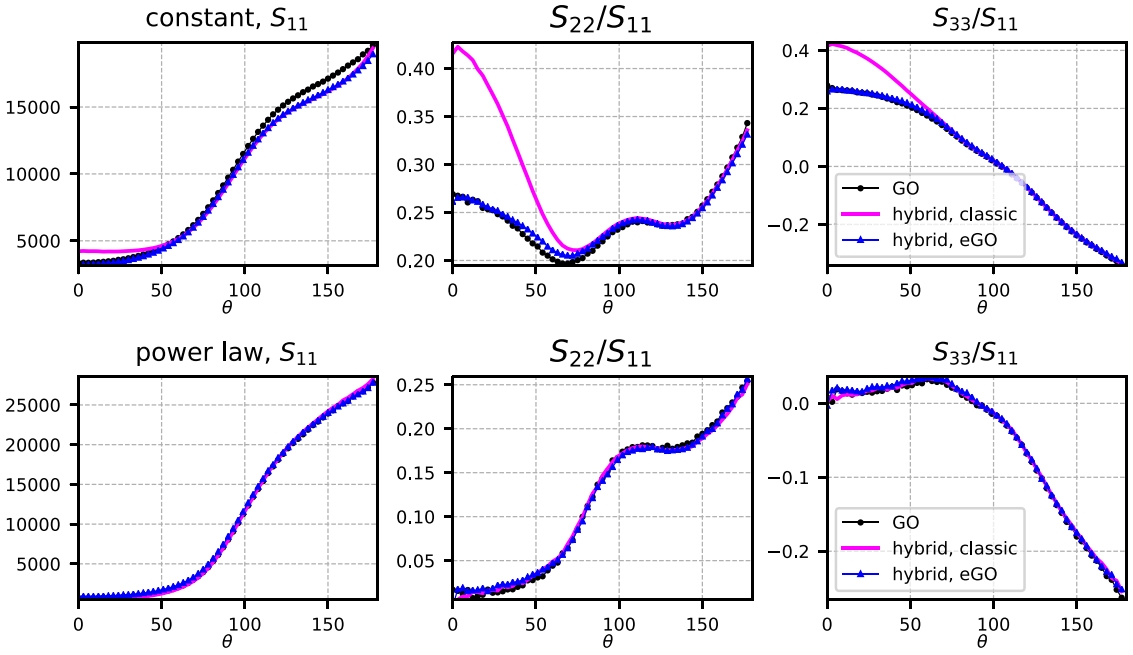

Fig. 14. Scattering elements S_{11}, S_{22} and S_{33} of Figs. 9 and 13 expanded to show the full scattering angle range.

inflated core smaller, the hybrid model would have a better match with the ground truth. The phase function would tilt to the correct position, and the maximum polarization would become higher. Additionally, the extinction distances are determined from the first-order scattering, which makes the initial configuration of the ray affect the distribution. If the second or third-order of scattering is used, the results could be improved.

The hybrid model will require more computing capacity due to the more rigorous computations in the mantle compared to the classical RT solution. The most demanding computation in this paper was the power-law size distribution (v=0.4) case in which 128 configurations were simulated in parallel. The mesh generation took around 8 hours, and an additional 12 hours were required to run the light scattering framework (17 000 rays). In comparison, the light scattering framework with the hybrid model was able to trace 30 000 rays in 12 hours without problems of convergence, whereas the pure RT approach method took around 30 minutes in total. The RT core enables the use of a faster ray-tracing algorithm, because it is easier to check the distance to the surface of the sphere instead of using the AABB-tree for ray-triangle inter-

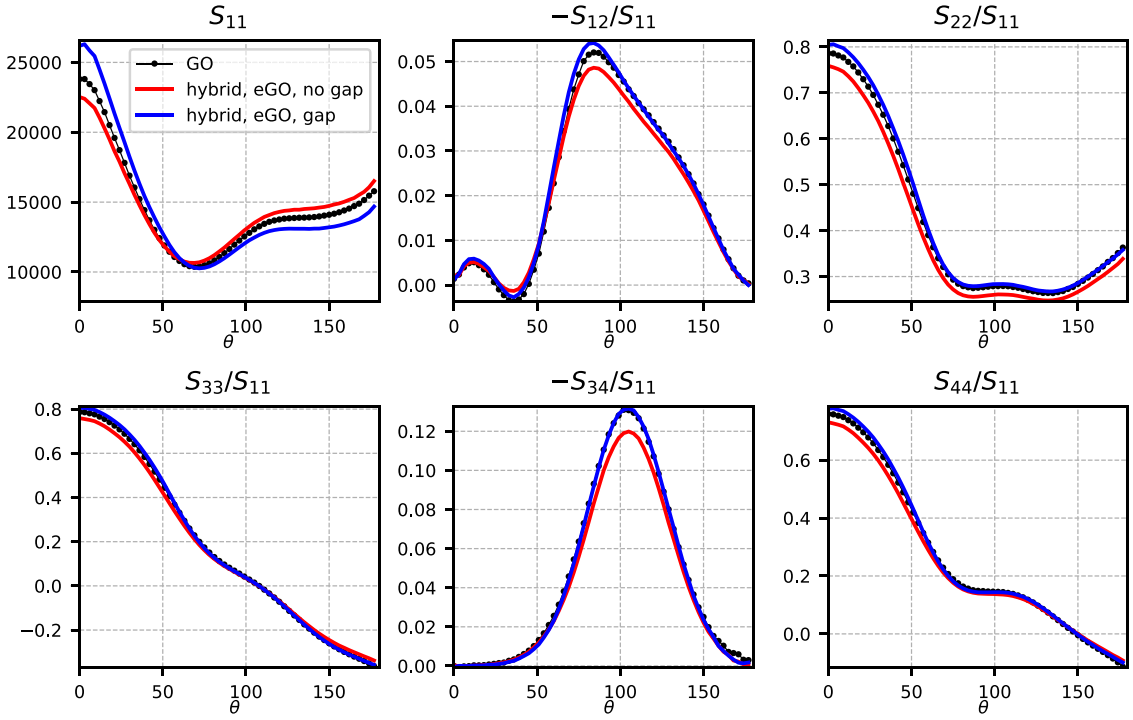

Fig. 15. Comparison of the effects of the gap to the results in Fig. 11.

section checks. An improved version of the new framework can be written by replacing the generalized ray-tracing functions with a more specialized ray-tracing engine.

There is also a question about the validity of the used mesh packing algorithm, but the light scattering characteristics obtained from the meshes, which were randomly placed (for v=0.1–0.3) or mechanically contracted (for v=0.3–0.4; e.g., compare Figs. 11, 12, and 13), do not show any worrisome trends due to the packing algorithm.

If the sparse medium is studied, the extinction distance distribution should be used, whereas dense media requires the hybrid model. The safest option would be to use the hybrid model with the extinction distance distribution in all of the cases, but if the mantle is thick and opaque enough, the underlying extinction rule in the RT core can have inaccuracies.

6. Summary

A new SIRIS4 framework was implemented in order to validate and create an approximation for multiple light scattering in multi-particle media in the geometric optics regime. The comparisons show that the radiative transfer approach can be improved for dense media by adding a mantle of discrete particles around diffusely scattering core and using the numerically acquired extinction distance distribution. The improved hybrid model will be a valuable asset for modeling planetary regoliths, which are out of reach for the pure geometric optics approaches due to computational complexity. The model can be improved by studying the behaviour of the extinction distance distribution more thoroughly and implementing a better characterization of the diffuse core.

Acknowledgments

We acknowledge Hannakaisa Lindqvist for the exceptional work with the SIRIS4 and Antti Penttilä for the discussions during the development of the new framework. We also thank reviewers for the insightful comments that helped to improve the paper. Computational resources were provided by CSC — IT Centre for Science Ltd, Finland, and FCGI – Finnish Grid and Cloud Infrastructure [36]. This work was supported by the Academy of Finland project 1325805.

References

[1] Schiffer R. The effect of surface roughness on the spectral reflectance of dielectric particles–Application to the zodiacal light. Astron Astrophys 1985;148:347–58.
[2] Mukai S, Mukai T, Giese RH, Weiss K, Zerull RH. Scattering of radiation by a large particle with a random rough surface. Moon Planet 1982;26:197–208. doi:10.1007/BF00929281.
[3] Peltoniemi JI, Lumme K. Light scattering by closely packed particulate media. J Opt Soc Am A 1992;9(8):1320–6. doi:10.1364/JOSAA.9.001320.
[4] Jacobowitz H. A method for computing the transfer of solar radiation through clouds of hexagonal ice crystals. J Quant Spectrosc Radiat Transf 1971;11(6):691–5. doi:10.1016/0022-4073(71)90047-1.
[5] Yang P, Liou K. An "exact" geometric-optics approach for computing the optical properties of large absorbing particles. J Quant Spectrosc Radiat Transf 2009;110(13):1162–77. doi:10.1016/j.jqsrt.2009.03.019.
[6] Bi L, Yang P, Kattawar GW, Hu Y, Baum BA. Scattering and absorption of light by ice particles: solution by a new physical-geometric optics hybrid method. J Quant Spectrosc Radiat Transf 2011;112(9):1492–508. doi:10.1016/j.jqsrt.2011.02.015.
[7] Sun B, Yang P, Kattawar G, Zhang X. Physical-geometric optics method for large size faceted particles. Opt Express 2017;25:24044. doi:10.1364/OE.25.024044.
[8] Grynko Y, Shkuratov Y, Förstner J. Light scattering by irregular particles much larger than the wavelength with wavelength-scale surface roughness. Opt Lett 2016;41(15):3491–4. doi:10.1364/OL.41.003491.
[9] Spencer GH, Murty MVRK. General ray-tracing procedureâ. J Opt Soc Am 1962;52(6):672–8. doi:10.1364/JOSA.52.000672.
[10] Dupertuis MA, Proctor M, Acklin B. Generalization of complex Snell–Descartes and Fresnel laws. J Opt Soc Am A 1994;11(3):1159–66. doi:10.1364/JOSAA.11.001159.
[11] Yang P, Gao B-C, Baum BA, Hu YX, Wiscombe WJ, Mishchenko MI, et al. Asymptotic solutions for optical properties of large particles with strong absorption. Appl Opt 2001;40(9):1532–47. doi:10.1364/AO.40.001532.
[12] Chang PC, Walker J, Hopcraft K. Ray tracing in absorbing media. J Quant Spectrosc Radiat Transf 2005;96(3):327–41. doi:10.1016/j.jqsrt.2005.01.001.
[13] Shkuratov Y, Petrov D, Videen G. Classical photometry of prefractal surfaces. J Opt Soc Am A 2003;20(11):2081–92. doi:10.1364/JOSAA.20.002081.
[14] Stankevich D, Shkuratov Y, Muinonen K. Shadow-hiding effect in inhomogeneous layered particulate media. J Quant Spectrosc Radiat Transf 1999;63(2):445–58. doi:10.1016/S0022-4073(99)00030-8.

[15] Muinonen K, Parviainen H, Naranen J, Josset J, Beauvivre S, Pinet P, et al. Lunar mare single-scattering, porosity, and surface-roughness properties with SMART-1 AMIE. Astron Astrophys Supp Ser 2011;531:A150. doi:10.1051/0004-6361/201016115.
[16] Wilkman O, Muinonen K, Videen G, Josset J-L, Souchon A. Lunar photometric modelling with SMART-1/AMIE imaging data. J Quant Spectrosc Radiat Transf 2014;146:529–39. doi:10.1016/j.jqsrt.2014.01.015.
[17] Muinonen K, Nousiainen T, Fast P, Lumme K, Peltoniemi J. Light scattering by Gaussian random particles: ray optics approximation. J Quant Spectrosc Radiat Transf 1996;55(5):577–601. doi:10.1016/0022-4073(96)00003-9.
[18] Muinonen K, Nousiainen T, Lindqvist H, Muoz O, Videen G. Light scattering by Gaussian particles with internal inclusions and roughened surfaces using ray optics. J Quant Spectrosc Radiat Transf 2009;110(14):1628–39. doi:10.1016/j.jqsrt.2009.03.012.
[19] Lindqvist H, Martikainen J, Räbinä J, Penttilä A, Muinonen K. Ray optics for absorbing particles with application to ice crystals at near-infrared wavelengths. J Quant Spectrosc Radiat Transf 2018;217:329–37. doi:10.1016/j.jqsrt.2018.06.005.
[20] Martikainen J, Penttilä A, Gritsevich M, Lindqvist H, Muinonen K. Spectral modeling of meteorites at UV–vis-NIR wavelengths. J Quante Spectrosc Radiat Transf 2018;204:144–51. doi:10.1016/j.jqsrt.2017.09.017.
[21] van de Hulst HC. Light Scattering by Small Particles; 1957.
[22] Bohren CF, Huffman DR. Absorption and Scattering of Light by Small Particles. New York: Wiley; 1983.
[23] Mishchenko M, Travis L, Lacis A. Multiple Scattering of Light by Particles: Radiative Transfer and Coherent Backscattering. Cambridge University Press; 2006. ISBN 9780521834902. https://books.google.fi/books?id=ODfEI-2ykLsC.
[24] Jackson JD. Classical Electrodynamics. 3rd ed. New York, NY: Wiley; 1999. ISBN 9780471309321. http://cdsweb.cern.ch/record/490457.
[25] Grynko Y, Shkuratov Y. Scattering matrix calculated in geometric optics approximation for semitransparent particles faceted with various shapes. J Quant Spectrosc Radiat Transf 2003;78(3):319–40. doi:10.1016/S0022-4073(02)00223-6.
[26] Williams S, Philipse A. Random packings of spheres and spherocylinders simulated by mechanical contraction. Phys Rev E Stat Nonlinear Soft Matter Phys 2003;67:051301. doi:10.1103/PhysRevE.67.051301.
[27] de Lange Kristiansen K, Wouterse A, Philipse A. Simulation of random packing of binary sphere mixtures by mechanical contraction. Physica A 2005;358(2):249–62. doi:10.1016/j.physa.2005.03.057.
[28] He D, Ekere N, Cai L. Computer simulation of the random packing of unequal particles. Phys Rev Stat Phys Plasmas, Fluids Related Interdiscip Topics 2000;60. doi:10.1103/PhysRevE.60.7098. 7098–104
[29] Pan J, Chitta S, Manocha D. FCL: A general purpose library for collision and proximity queries. In: 2012 IEEE International Conference on Robotics and Automation; 2012. p. 3859–66. doi:10.1109/ICRA.2012.6225337.
[30] Dupertuis MA, Acklin B, Proctor M. Generalized energy balance and reciprocity relations for thin-film optics. J Opt Soc Am A 1994;11(3):1167–74. doi:10.1364/JOSAA.11.001167.
[31] The CGAL Project. CGAL User and Reference Manual. 413. CGAL Editorial Board; 2018. https://doc.cgal.org/4.13/Manual/packages.html.
[32] Hansen JE, Travis LD. Light scattering in planetary atmospheres. Space Sci Rev 1974;16:527–610. doi:10.1007/BF00168069.
[33] Macke A, Mishchenko MI, Cairns B. The influence of inclusions on light scattering by large ice particles. J Geophys Res 1996;101:23311–16. doi:10.1029/96JD02364.
[34] Nousiainen T, Lindqvist H, McFarquhar GM, Um J. Small irregular ice crystals in tropical cirrus. J Atmosp Sci 2011;68(11):2614–27. doi:10.1175/2011JAS3733.1.
[35] Muinonen K, Stankevich D, Shkuratov Y, Kaasalainen S, Piironen J. Shadowing effect in clusters of opaque spherical particles. J Quant Spectrosc Radiat Transf 2001;70:787–810. doi:10.1016/S0022-4073(01)00046-2.
[36] Finnish Grid and Cloud Infrastructure, urn:nbn:fi:research-infras-2016072533. 2019.